Comparison Between Geometrical Shapes for New Designs of Split Ring Resonators

Thill A. Kadhum Al-Musawi

Physics Department, Science College, Al-Muthanna University, Iraq

Corresponding author: ***thillakeel@mu.edu.iq***

Received 19 Nov. 2024, Accepted 4 Dec. 2024, published 30 Dec. 2024.

DOI: 10.52113/2/11.02.2024/131-139

Abstract: In electromagnetics, the material's characteristics can be defined by the permittivity, permeability, and conductivity of different ranges of frequencies, where the refractive index and the impedance can be extracted. In this work, the properties of artificial metamaterials were studied by designing a unit cell of three-dimensional lattice vectors using CST (Computer Simulation Technology). A simulation process was employed to obtain the S-parameters, and the magnetic resonance frequency of several Split Ring Resonators (SRRs) was investigated. Also, the work introduced four new designs of srr, circl-square (c-sq), circl-square-circl resonator (c-sq-c), square-circle resonator (sq-c), and square-circle-square resonator (sq-c-sq). Conventional SRR structures faced challenges operating effectively at higher frequencies due to production difficulties. Scaling down the structure results in narrow split and gap regions, potentially leading to contact issues between metallic regions. Traditional SRR structures were limited to operating within a few gigahertz frequency ranges. SRR structures exhibited electrical resonance for different polarisations and propagation directions. The new design showed a negative response within the (7-12) GHz range and a negative refracted index ranging from (-4.35 to -5.6)**.**

Keywords: Effective permeability, Effective permittivity, S- parameters, refractive index, metamaterials.

1. Introduction

SRRs and conducting wires are applied to creating metamaterials with negative permeability and permittivity, respectively, so, the negative permittivity is realised using conducting wires, and negative permeability can be realised using split ring resonetors SRR [1], the NIM can be realized by periodically aligning structures that exhibit both negative permeability and negative permittivity, this means arranging the SRRs and conducting wires in a periodic lattice to create the desired metamaterial. The unit cell is the basic building block of the metamaterial, it contains a combination of SRRs for negative permeability and conducting wires for negative permittivity [6- 8]. Complex transmision and reflaction characteristics of the propased SRR are obtain by CST MS, and then they are used to extricate the effective medium parameters ϵ_{eff} and μ_{eff} of the designed metamaterials to verify the nature of resulting resonance [9- 11].

The negative permittivity is realised using conducting wires, and negative permeability can be realised using split-ring resonators (SRRs) [1], where the negative index materials (NIMs) can be realised using periodic alignments of structures exhibiting negative permittivity and negative permeability [2-5]. All four geometrical configurations of the SRR, presented on similar dielectric substrates, are studied with the same physical dimensions. The comparison of their resonance frequency, which determines the region of negative permeability, is provided [6-8]. Complex transmission and reflection characteristics of the proposed SRR were obtained by CST MS, and then they were used to extract the effective medium parameters ϵeff and μeff of the designed metamaterials to verify the nature of the resulting resonance.

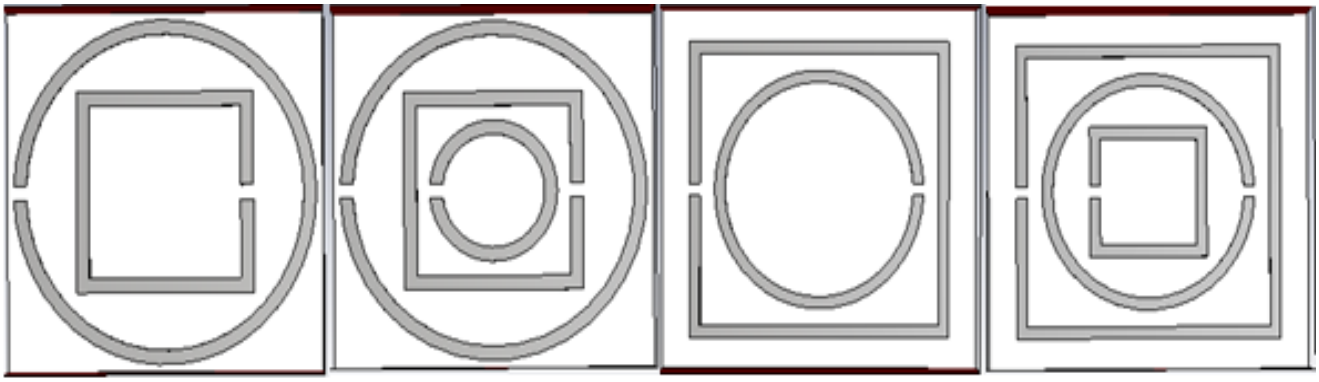

Fig. (1): A typical unit cell SRR with a metellic one rod placed on the dielectric board for (c- sq) SRR design, (c- sq- c) SRR design, (sq- c) SRR design and (sq- c- sq) SRR design.

2. Methodology

2.1. Design and Simulation

The resonanc frequency for SRR of different geometries is computed using equations 1 and 2 [11]:

$$C = \frac{\epsilon a t}{2g} \qquad (1)$$

$$L = \frac{\mu_0 b}{\sqrt{\pi}}\left[\log\left(\frac{32b}{a\sqrt{\pi}}\right) - 2\right] \qquad (2)$$

where L is the equivalent induced inductance, μ is the permeability of free space, a is the ring width, g is the split gap, C is the total series capacitance between the rings, ϵ is the permittivity of the material, b is the ring length, and t is the thickness of the splintering. The dimensions are chosen to be a = 0.1 mm, g = 0.1 mm, b = 2.5 mm, and t = 0.25 mm. Capacitors and inductors in parallel act as a resonant circuit with a resonance frequency.

The simulated resonance frequency was extracted from the transmission coefficient e curves. These results demonstrate that a desired number of magnetic resonance can be realised by selecting the number of SRR rings within the limits of geometrical constraints, where the (c-sq) SRR resonates at a higher refrequency compared to the other designs and at a lower refrequency compared to the (sq-c) SRR, having similar dimensional parameters, as in Table 1 [12].

Results

3.1. Design and Simulation

2. Design and Simulation

After the proper designs are completed, it concluded that the frequencies effective range that contains the dips and peaks under interest is between (8- 12) GHz as in Figures (2) to (5). This relationship between the number of rings and resonant frequency could provide valuable for optimizing the design of these metamaterials.

From the real parts parameters for S11 and S21, the effective resonence frequencies for all designs have been found as in table 1, that the resonant frequency increases as the number of rings decreases for all four designs, based on the real parts parameters for S11 and S21.

This relationship between the number of rings and resonant frequency could provide valuable for optimizing the design of our metamaterials. It makes that decreasing capacitance, which happens when the gap distance between the rings increases, leads to a higher resonant frequency.

The inverse relationship between capacitance and resonant frequency is a key factor in the design of metamaterials. From the results, the conclusion that the design with the largest resonant frequency is (c-sq), followed by (c-sq-c), (sq-c- sq), and (sq-c) provides valuable into how these configurations affect responses.

After completing the proposed designs, it was concluded that the effective range of frequencies that contains the peaks and dips under interest was between (8-12) GHz, as shown in Figures (2) to (5). From the real parts of the S11 and S21 parameters, the effective resonance frequencies for all designs were found as illustrated in Table 1, and it was obvious that the resonant frequency was directly proportional to the decreasing number of rings for all four designs. This occurs due to decreasing the capacitance that is inversely proportional with increasing the gap distance between the rings. It can be concluded that the largest value of resonant frequency was for the design (c-sq) and then (c-sq-c), (sq-c), and (sq-c-sq).

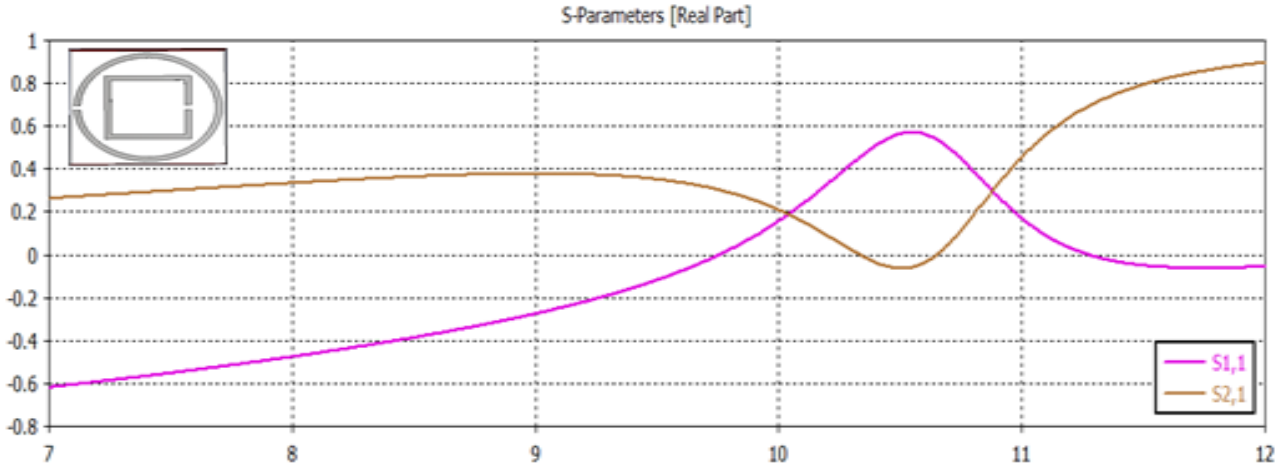

Fig. (2): Real parts of S11 and S21 parmeters for (c- sqdesign.

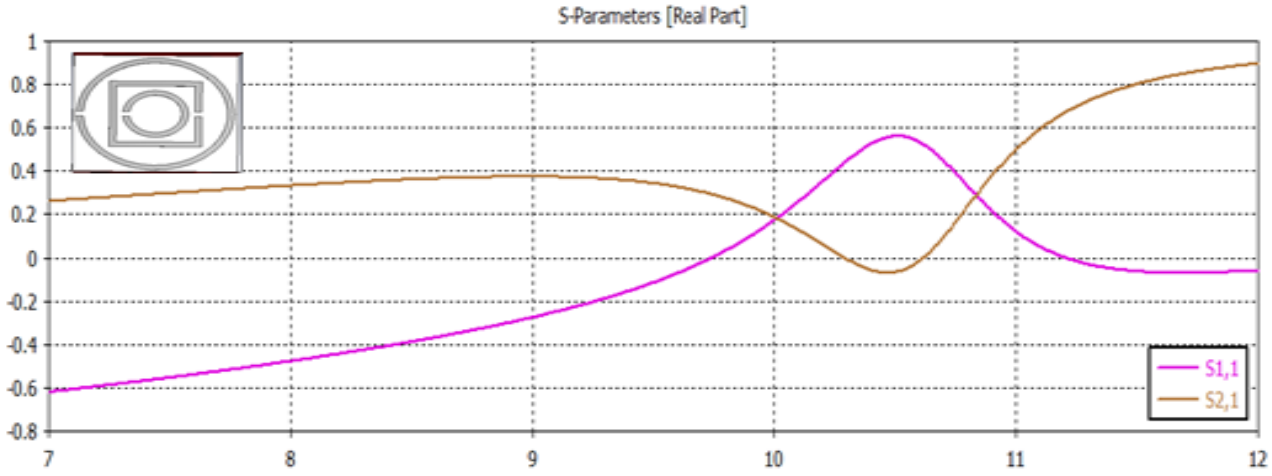

Fig. (3): Real parts of S11 and S21 paremeters for (c- sq- c) desegn.

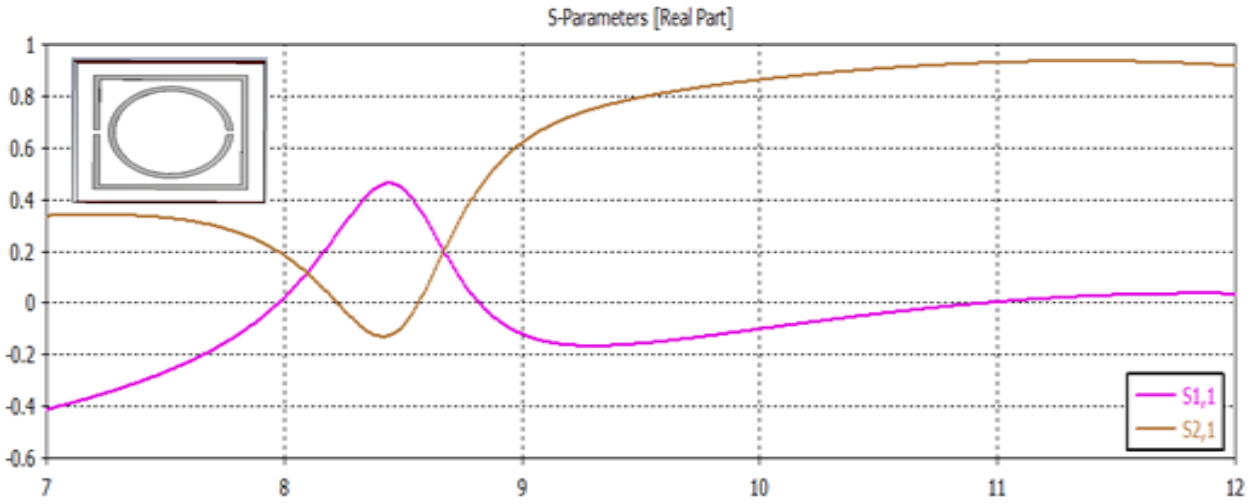

Fig. (4): Real parts of S11 and S21 paremeters for (sq- c) design.

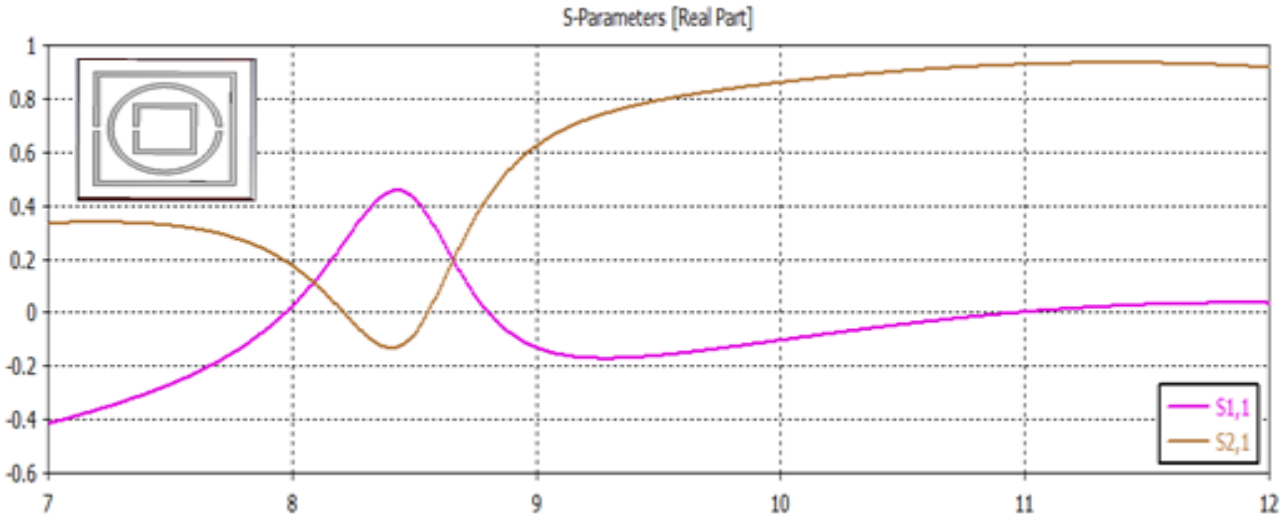

Fig. (5): Real parts of S11 and S21 paremeters for sq- c- sq design.

Then, the values of real ϵ of the design were extracted from S11 and S21 using post-processing of CST. It was obvious that the negative values of ϵreal were found in the frequencies below 12 GHz. Also, the negative values of μreal were estimated using the same manner, and it seems that these values shifted to the right (higher frequency or shorter wavelength) as the number of rings decreased, as exhibited in Figure 6.

Then, the values of real of ϵ of design have been extrected from S11 and S21 using post- processing of CST. It is obvious that the negative values of ϵ_{real} were found in the frequencies below 12 GHz. Also, the negative values of μ_{real} have been estimated using the same mannere and it seems that these values shiftted to the right (higher frequency or shorter wavelength) as rings number decrease, as exhibited in Figure 6.

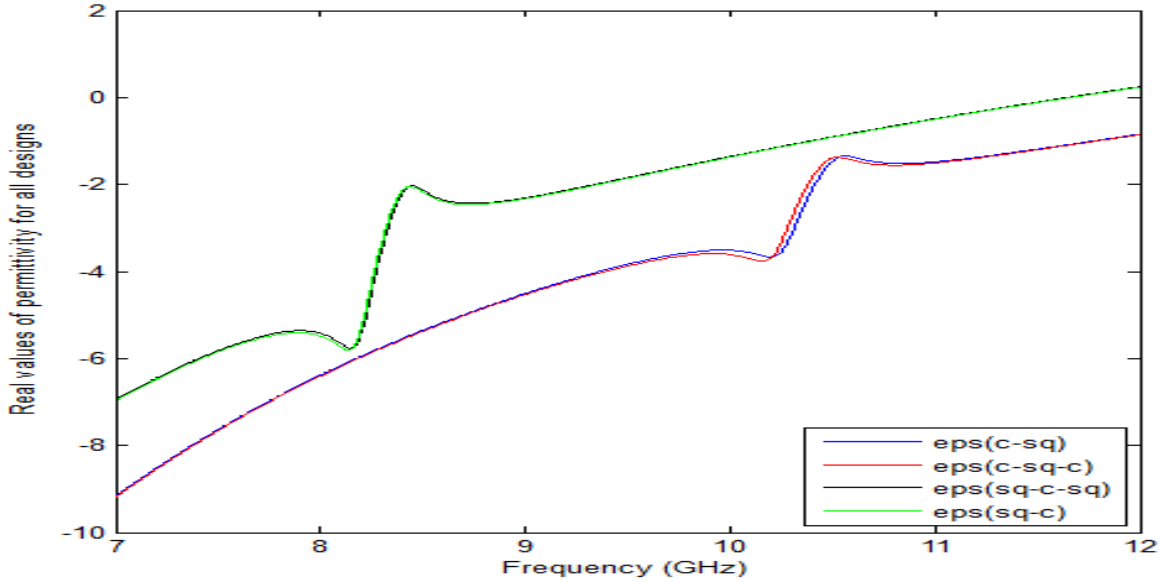

Fig. (6): Real parts of ermittivity ϵ paremeters for all designs.

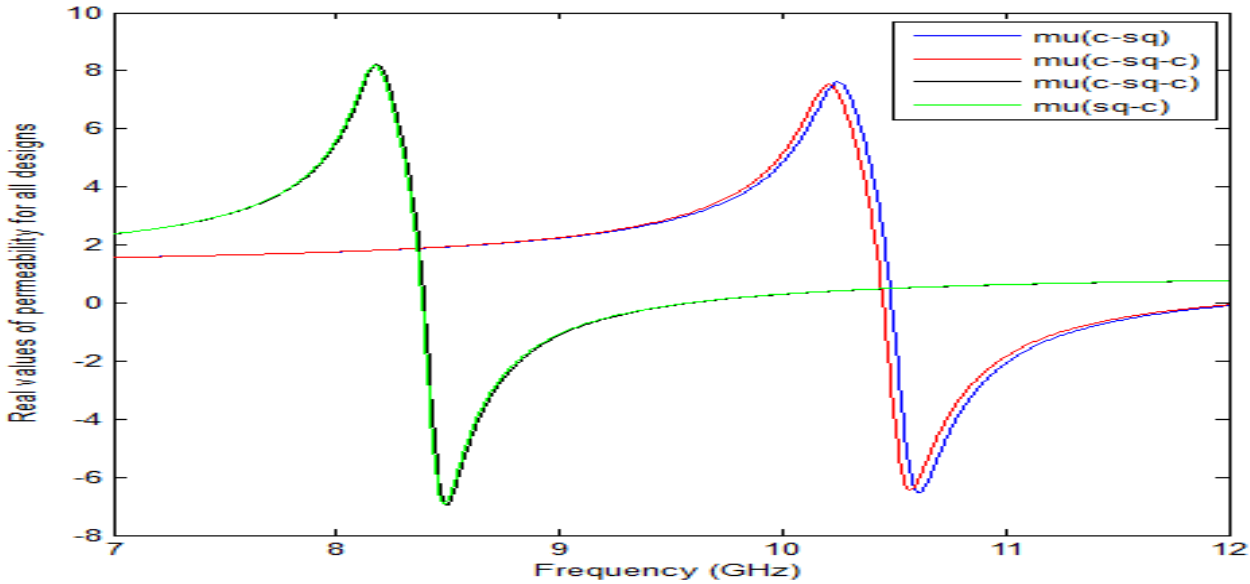

Fig. (7): Real parts of permebility μ paremeters for all designs.

From Figure 8, it can be concluded that the largest value of effective refractive index is for the design (c-sq) SRR and then (c-sq-c) SRR, (sq-c-sq) SRR and (sq-c) SRR, and n_{eff} exhibits a negative values Table 1.

Whene examing Figure 8 it can be concluded that the largest value of effective refrective indix was for the desegn (c- sq) and then (c-sq-c), (sq-c) and (sq-c-sq), and neff exhhibits a negetive values Table 1.

Table 1: Comparison of computed and simulated resonance frequencies.

Type of SRR	SRR Resonance frequency (GHz)		Effective refractive indix (n_{eff})
	f s11	f s22	
c-sq	10.550	10.505	-4.35- 0
c-sq-c	10.510	10.465	-4.4- 0
sq-c-sq	8.440	8.415	-5.5- 0
sq-c	8.430	8.405	-5.6- 0

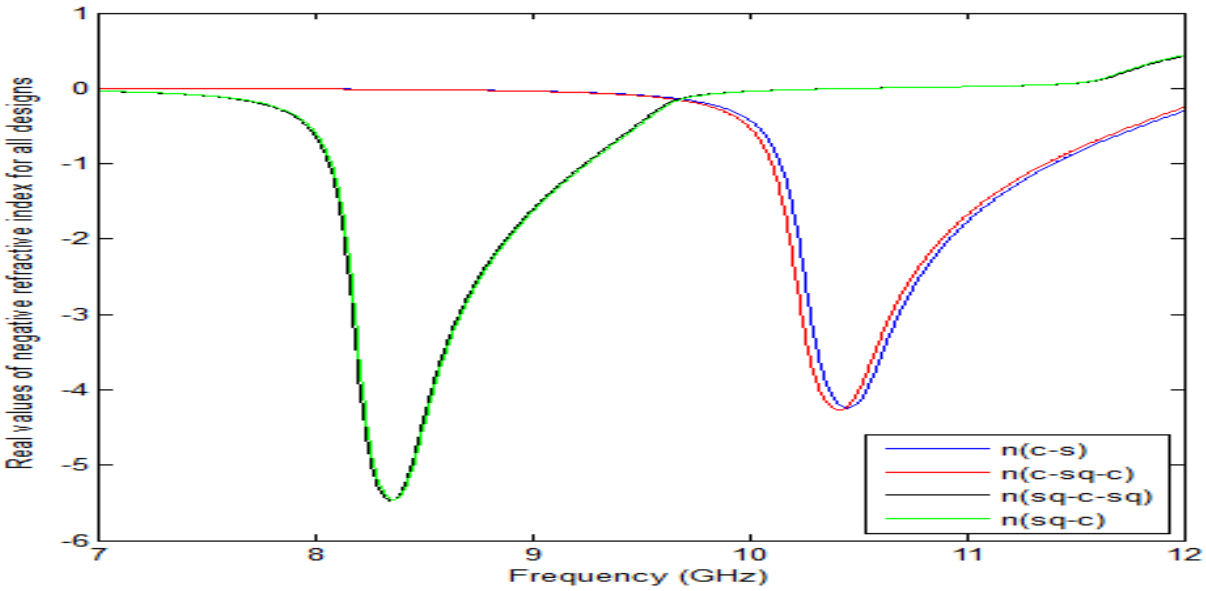

Fig. (8): Effective refractive indix n_{eff} for all designs.

4. Discussion

The thorough analysis to the designs by printing all four geometrical designs of the SRRs on similar dielectric substrates and studying them under identical physical dimensions. Verifying the resonance behavior through both measurements and modeling transmission via a single SRR unit cell ensures that our findings are robust and reliable. Comparing the resonance frequencies to determine the region of negative permeability is crucial for understanding the behavior of left-handed LH media. Using the S- parameters along with the magnetic permeability $\boldsymbol{\mu_{eff}}$ and electric permittivity $\boldsymbol{\epsilon_{eff}}$ data to calculate the effective refractive index $\mathbf{n_{eff}}$ provides a complete picture of the metamaterials' properties. The effect of the rods addition on the S11 and S21 parameters was studied at broadb and (7- 12) GHz, and the values of real of $\boldsymbol{\epsilon_{eff}}$ and μeff were extracted from S- parameters. Then, every rod's effective resonance frequency was determined, as shown in table (1). From the results that the (tr-tr) SRR design has the largest effective refractive index $\mathbf{n_{eff}}$, followed by the (c-tr) and (sq-tr) SRR designs. This also correlates with the largest resonant frequency being observed in the (tr-tr) SRR design and then (c- tr) and (sq- tr) SRR as in Table (1). These findings provide a clear hierarchy of performance among the designs, which can be extremely useful for optimizing and applying these metamaterials. The observation that ϵ real shows negative values below 12 GHz suggests the presence of negative permittivity within that frequency range, which is a hallmark of metamaterials exhibiting left- handed behavior. Similarly, our findings indicate that the negative values of μ_{real} shift to higher frequencies (or shorter wavelengths) as the number of rings decreases which provide a valuable insight into how the magnetic resonance is influenced by the design. This can be critical for applications where precise control over electromagnetic properties is required.

5. Conclusion

All four geometrical designs of the SRRs printed on similar dielectric substrates were studied in the same physical dimensions. These resonators' resonance behaviour was verified by measuring and modelling transmission via a single SRR unit cell. The comparison of their resonance frequency was performed, which determines the region of negative permeability. Finally, the S-parameters, together with the magnetic permeability μeff and electric permittivity ϵeff data, were used to calculate the effective refractive index neff of LH media for the different designs. The effect of the rods addition on the S11 and S21 parameters was studied broadly (6-24 GHz), and the values of real ϵeff and μeff were extracted from S-parameters. Then, every rod's effective resonance frequency was determined, as shown in table (1). From the analysis of the results of the study in Table (1), it can be concluded that the largest value of the effective refractive index

is for the design (tr-tr) SRR and then (c-tr) and (sq-tr) SRR. Therfore that the largest value of resonant frequency was for the desegn (tr-tr) SRR and then (c-tr) and (sq-tr) SRR as illustrated in Table (1).

References

[1] Saha, C., and Siddiqui, J.Y., 2011, A Comparative Analyis for Split Ring Resonators of Different Geometrical Shapes, IEEE, 2011, 1-4, doi: 10.1109/AEMC.2011.6256871, 2011.

[2] Waqas, M., Akbar, Z., Saeed, M.A., khan, M., 2014, Rectangular Split Ring Double Negative Metamaterial having Simultaneous Negative Permittivity and Permeability, Advanced Computational Techniques in Electromagnetics, 1-8, doi:10.5899/2014/acte-00178, 2014.

[3] He, X., Qiu, L., Wang, Y., Geng, Z,, Wang, J. and Gui, T., A Compact Thin-Film Sensor Based on Nested Split-Ring-Resonator (SRR) Metamaterials for Microwave Applications, Journal of Infrared, Millimeter and Terahertz Waves, 32, 902-913, doi: 10.1007/s10762-011-9807-4, 2011.

[4] Nornikman, H., Ahmad, B. H., Abd Aziz, M. Z. A., Othman, A. R., Effect of Single Complimentary Split Ring Resonator Structure on Microstrip Patch Antenna Design, ISWTA, 239- 244, Indonesia, 2012.

[5] Al-musawi, T.A.K., Mahdi, S.A. and AL-Asadi S. Y., CHARACTERISTICS OF CIRCLE- SQUARE SRR LEFT HANDED MATERIALS, Journal of optoelectronics laser, 41, **7**, doi: 10050086.2022.07.123, 2022.

[6] Mahmud, M.Z., Islam, M. T., Misran, N., Singh, M.J. and Mat, K., 2017, A Negative Indix Metamaterial to Enhance the Performance of Miniaturized UWB Antenna for Microwave Imaging Applications, Appl. Sci., 7, 1149, doi:10.3390/app7111149, 2017.

[7] Hindy, M. A., ElSagheer, R. M. and Yasseen, M. S., 2017, A Circular Split Ringe Resonator (CSRR) Left Handed Metamaterial (LHM) having Simultaneous Negative Permeability and Permittivity, International Journal of Hybrid Information Technology, 10, 1, 171-178,.

[8] Salim, A., and Lim, S., 2016, Complementary Split-Ring Resonator-Loaded Microfluidic Ethanol Chemical Sensor, Sensors, 16, 1802, doi:10.3390/s16111802, 2016.

[9] Zerrouk, Z., Setti, L., 2020, Effect of Circular Split Ring Resonator Array on Circular Microstrip Antenna Used for Intelligent Transportation System (ITS), IJSR, 9, 6, doi: 10.21275/SR20528190814 ,.

[10] Numan, A. B., and Sharawi, M. S., 2013, Extraction of Material Parameters for Metamaterials Using a Full-Wave Simulator, IEEE Antennas and Propagation Magazine, 55, 5.

[11] Turkmen, O., Ekmekci, E., and Turhan-Sayan, G., 2011, A New Multi-ring SRR Type Metamaterial Design with Multiple Magnetic Resonances, Journal of Infrared, Millimeter and Terahertz Waves, Springer, 902-913, doi: 10.1007/s10762-011-9807-4.

[12] Hadkar, N., Jagtap, S., 2015, Design of Square Shaped Miniaturized Split Ring Resonators, Journal of Engineering Research and Applications, 5, 5, 11- 14,.

[13] Patel, S.K. and Argyropoulos, C., 2016, Enhanced bandwidth and gain of compact microstrip antennas loaded with multiple corrugated split ring resonators, Journal of Electromagnetic Waves and Applications, doi: 10.1080/09205071..1167633, 2016.

[14] Al-Musawi, T.A.K., Mahdi, S.A., AL-Asadi, S.Y., 2021, Characteristics of Left Handed Materials, NeuroQuantology, 19, 11, doi: 10.14704/nq.2021, 2021.